Desalination and Water Treatment
www.deswater.com

1944-3994/1944-3986 © 2012 Desalination Publications. All rights reserved
doi: 10/5004/dwt.2012.2561

39 (2012) 55–69
February

Taylor & Francis
Taylor & Francis Group

On the induction time of $CaCO_3$: effect of ionic strength

Tarek Waly[a,b,c,*], Maria D. Kennedy[a,b], Geert-Jan Witkamp[b], Gary Amy[a,b], Jan C. Schippers[a]

[a]*UNESCO-IHE, Delft, The Netherlands*
[b]*TUDelft, Delft, The Netherlands*
[c]*Dow Chemicals, UAE*
Tel. +31634051245; Fax: +31152122921; email: t.waly@delft-environment.net, t.waly@unesco-ihe.org

Received 30 December 2010; Accepted 27 February 2011

ABSTRACT

This research investigated the induction times of $CaCO_3$ as a function of the saturation and ionic strength for synthetic solutions based on the Gulf of Oman seawater analysis. The investigation aimed to determine at elevated ionic strength levels, (i) the $CaCO_3$ phase incorporated in the Stiff and Davis saturation index and (ii) the mechanism of nucleation involved. Induction time experiments were performed with synthetic concentrates having different ionic strengths of 0.054, 1.12, 1.34, 1.61 mole/l. Results showed that S&DSI incorporate the solubility of calcite at low ionic strength but vaterite for high ionic strength water. This expectation was confirmed with microscopic analysis of the formed crystals at the end of the induction time experiments (24 h) as vaterite was found in the solution instead of calcite. These findings indicate that vaterite and not calcite maybe the precipitating phase in seawater. The study of the mechanism of nucleation showed three different trends describing three different nucleation mechanisms; namely homogenous, heterogeneous and a one characterized by an intermediate surface tension. The calculations of the apparent surface energy showed values ranging from 15–94 mJ/m^2 which is consistent with literature data for vaterite. Results suggest that for the level of saturation reached in SWRO systems, the nucleation mechanism will most probably be heterogeneous.

Keywords: Nucleation; Membrane; Desalination; Surface energy; Phase; Seawater

1. Background

1.1. Introduction

In seawater reverse osmosis (SWRO) plants where 25–50% of the seawater is converted into fresh water, scaling problems are considered a constant potential in plant design and operation. There are many types of scale that may form in a plant, but the most common scalants in SWRO are $CaCO_3$ and Mg $(OH)_2$ (second pass). Pretreatment using acid is widely used for $CaCO_3$ scaling prevention in SWRO plants. For the purpose of optimizing acids doses, solution stability after its saturation limits are exceeded (induction time) need to be studied [1]. The aim of this research is to determine the effect of salinity on the induction time of $CaCO_3$ in SWRO concentrates.

Seawater salts mainly comprise 7 main ions: Ca^{2+}, Mg^{2+}, Na^+, K^+, Cl^-, HCO_3^- and SO_4^{2-} as shown in Table 1. The pH of the seawater usually ranges between 7.8 (e.g., the Red Sea) to 8.3 (e.g., the Atlantic Ocean). Lower pH values (<7.8) may be found if beach wells are the main feed water source.

1.2. Solubility of salts

When an ionic compound is added to water, it will usually dissolve in the solution as its ions and complexes. If the activity of an ionic compound added to a volume

---

*Corresponding author.

Table 1
Seawater composition (intake of desalination plant in the Gulf of Oman)

	Parameter	Average	Unit
Anions	Calcium	474	mg/l
	Sodium	12,244	mg/l
	Potassium	434	mg/l
	Magnesium	1356	mg/l
Cations	Alkalinity total as $CaCO_3$	120	mg/l
	Carbonate	23	mg/l
	Phosphate	0.1	mgP/l
	Silicate	0.13	mg/l
	Chloride	21,535	mg/l
	Sulphate	2772	mg/l
Physiochemical properties	Conductivity	60	mS/cm
	Hardness non carbonate($CaCO_3$)	6718	mg/l
	Hardness total ($CaCO_3$)	6838	mg/l
	pH	8.1	
	Density	1.03	g/cm^3
	TDS	39,017	mg/l
	Ionic strength	0.76	mole/l

is in excess, an equilibrium is reached when the number of ions entering the solution from the solid compound is equal to the number of ions leaving the solution to the solid compound according to the following reaction represented in Eq. (1) [2]:

$$CaCO_3 \rightleftharpoons Ca^{2+} + CO_3^{2-} \tag{1}$$

The first requirement for precipitation or scale formation is supersaturation of the solution with respect to the scaling salt. If the solubility is exceeded based on the maximum amount of salt soluble in a solution (at a given temperature) precipitation may occur [3–5]. The equilibrium thermodynamic solubility product (K_{sp}) varies with temperature wherein alkaline scale solubility decreases as the temperature increases [6]. It is also noted that the rate of scaling may be enhanced by surface roughness, hydraulic conditions, as well as the surface charge [7].

1.3. Common methods used to determine the precipitation potential of $CaCO_3$

In seawater, $CaCO_3$ saturation is calculated by the use of different indices such as the Stiff & Davis Stability Index (S&DSI) [8]; the Saturation Index (SI) and the Saturation Ratio (S_a). These indices were developed to predict the possibility of sparingly soluble salts precipitation, except S&DSI which is developed specifically for $CaCO_3$.

1.4. Stiff and Davis Stability Index (S&DSI)

Developed in 1952, the S&DSI is widely used for calcium carbonate scaling potential in higher ionic strength solutions similar to that of sea water (Eqs. 2 and 3) [8,9]:

$$\text{S\&DSI} = \text{pH} - \text{pH}_3 \tag{2}$$

$$\text{pH}_3 = \text{pCa} + \text{pHCO}_3^- + k \tag{3}$$

where pHs is the saturation pH , pCa is the $-\text{Log}_{10}$ Ca, pHCO_3^- is the $-\text{Log}_{10}$ HCO_3^- and k is a factor compensating for salinity and temperature.

The S&DSI was developed after experimental work to take into account the ionic strength in saturation calculations. The ionic strength limit in the S&DSI index ranges between 0–3.6 mole/l and is limited to temperature ranges from 0 °C to 50°C, making it a very useful tool for calcium carbonate scaling determination in seawater reverse osmosis systems [9]. A positive S&DSI indicates the tendency to form calcium carbonate scale, while a negative value indicates no tendency for scaling formation [9]. One of the main problems of this index is that it cannot be extrapolated out of its salinity and temperature ranges.

Stiff & Davis carried out their experiments at different levels of ionic strength and at three temperatures, namely 0, 30, 50°C. The advantage of this technique is that it incorporates the change dissociation constants due to the increase in temperature and salinity. Although not known, the solubility product of the precipitating phase is incorporated in *k* value of the S&DSI. A main disadvantage of using S&DSI that it ignores the effect of seawater salts other than NaCl e.g., Mg^{2+}, SO_4^{2-}, K^+, etc. which may affect the accuracy of the predicted saturation using S&DSI [9].

1.5. Saturation index (SI)

This saturation index predicts the scaling potential of sparingly soluble salts taking into consideration the interaction between ions. The index incorporates the activity coefficients in its activity calculations which takes into account the effect of ionic complexation due to high salinity (Eqs. 4–7). For SWRO concentrates it is preferable to use Pitzer model rather than Davis or extended Debye Huckel models in calculating the activity coefficients as the former takes into account the ionic specific interaction [1,10–15]:

$$\mathrm{SI} = \mathrm{Log}\left(\frac{[\mathrm{Ca}^{2+}]\gamma_{\mathrm{ca}^{2+}}[\mathrm{CO_3}^{2-}]\gamma_{\mathrm{CO_3}^{2-}}}{K_{\mathrm{sp}}}\right) \tag{4}$$

$$\mathrm{pH} = -\mathrm{Log}[\mathrm{H}]\gamma_{\mathrm{H}^+} = \mathrm{p}K_{a2} + \log\frac{[\mathrm{CO_3}^{2-}]\gamma_{\mathrm{CO_3}^{2-}}}{[\mathrm{HCO_3}^{-}]\gamma_{\mathrm{HCO_3}^{-}}} \tag{5}$$

$$\mathrm{SI} = \mathrm{Log}\left(\frac{[\mathrm{Ca}^{2+}]\gamma_{\mathrm{ca}^{2+}}K_{a2}[\mathrm{HCO}_3^{2-}]\gamma_{\mathrm{HCO}_3^-}}{K_{\mathrm{sp}}[\mathrm{H}]\gamma_{\mathrm{H}^+}}\right) \tag{6}$$

$$\begin{aligned}\mathrm{SI} = \mathrm{pH} - (&\mathrm{p}[\mathrm{Ca}^{2+}] + \mathrm{p}[\mathrm{HCO}_3^-] \\ &+ \mathrm{p}K_{a2} - \mathrm{p}K_{\mathrm{sp}} + \mathrm{p}\gamma_{\mathrm{ca}^{2+}} + \mathrm{p}\gamma_{\mathrm{HCO}_3^-})\end{aligned} \tag{7}$$

where K_{sp} is the solubility product of $CaCO_3$, $\gamma_{\mathrm{ca}^{2+}}$, $\gamma_{\mathrm{CO}_3^{2-}}$, $\gamma_{\mathrm{HCO}_3^-}$, and γ_{H^+} are the activity coefficients of calcium, carbonate, bicarbonate and hydrogen, respectively, log X is $\log_{10}X$, K_{a2} is the second acidity constant and K_{sp} is the thermodynamic solubility product.

When compared to S&DSI (Eqs. 8 and 9)?

$$\mathrm{S\&DSI} = \mathrm{pH} - (\mathrm{p}[\mathrm{Ca}^{2+}] + \mathrm{p}[\mathrm{HCO}_3^-] + k \tag{8}$$

$$k = -\mathrm{p}K_{\mathrm{sp}} + \mathrm{p}K_{a2}^{T} + \mathrm{p}\gamma_{\mathrm{Ca}^{2+}} + \mathrm{p}\gamma_{\mathrm{HCO}_3^-} \tag{9}$$

1.6. Saturation ratio (S_a)

Although S_a is less widely used when compared to the SI, it adopts the same concept for saturation calculations as shown in Eqs. 10 and 11 [1].

$$S_a = \frac{[\mathrm{Ca}^{2+}]\gamma_{\mathrm{ca}^{2+}}[\mathrm{CO}_3^{2-}]\gamma_{\mathrm{co}_3^{2-}}}{K_{\mathrm{sp}}} \tag{10}$$

Values of S_a greater than one mean that it is more likely that the salt will scale while values less than one mean that the solution is undersaturated with respect to this specific salt [1].

$$\mathrm{SI} = \mathrm{Log}\, S_a \tag{11}$$

1.7. Mechanism of nucleation

The mechanism of nucleation is divided into homogenous or heterogeneous nucleation [16]. Homogeneous nucleation is where the formation of the solid phase is not influenced by the presence of any solid phase, and heterogeneous nucleation is where the formation of new solid phase particles is catalyzed by the presence of a foreign solid phase [1]. The formed nucleus grows further to the crystalline phase while the formation of stable crystals needs an aging step for the formation of the final product [17].

1.8. Homogenous nucleation

For the formation of a solid phase cluster comprising N molecules and having surface A_N, the change of Gibbs energy accompanying this change can be defined as showed in Eq. 12 [1]:

$$\Delta G_{\mathrm{hom}} = -N\phi + A_N\gamma_{\mathrm{S}} = \frac{k_v r^3}{\vartheta}\phi + K_a r^2 \gamma_{\mathrm{S}} \tag{12}$$

where ΔG_{hom} is the change in Gibbs energy in the homogenous zone, N is the number of molecules, A_N is the nuclei surface area γ_s represents the surface energy, φ is the affinity (Eq. 20), K_v volume geometric factor (equals 1 for cubic shapes), K_a area geometric factor (equal 1 for cubic shapes), θ molecular volume and r is the nuclei radius.

Evaluating the critical radius in the equation of the Gibbs free energy gives the maximum free Gibbs energy (also called energy barrier), in which the probability of its growth and its decay are equal (Eq. 13) [1]:

$$\frac{\mathrm{d}\Delta G_{\mathrm{hom}}}{\mathrm{d}N} = -\phi + \frac{A_N}{\mathrm{d}N}\gamma_{\mathrm{S}} = 0 \tag{13}$$

And the critical radius r_{crit} in such cases is found as shown in Eq. 14:

$$r_{\text{crit}} = \frac{2\vartheta k_a \gamma_S}{3k_v \phi} \tag{14}$$

By substitution and rearrangement:

$$\Delta G_{\text{hom}}^{\text{max}} = \frac{\beta \vartheta^2 \gamma_S^3}{\phi^2} \tag{15}$$

Thus, using the geometrical (area and volume) constants K_a and K_v, the geometric expression β can be expressed as shown in Eq 16:

$$\beta = \frac{4k_a^3}{27k_v^2} \tag{16}$$

And consequently the number of molecules forming the critical nuclei can be written as in Eq. 17:

$$N = \frac{V}{\vartheta} = \frac{k_v r^3}{\vartheta} = \frac{2\beta\vartheta^2\gamma_S^3}{\phi^3} \tag{17}$$

where V is the nuclei volume which can be related to the supersaturation (S_a) as in Eq. 18:

$$\phi = \nu k_b T Ln S_a \tag{18}$$

And the rate of nucleation (J) in such cases can be written as follows:

$$J = \Omega_{\text{hom}} \exp\left(\frac{-\Delta G_{\text{hom}}}{k_b T}\right) = \Omega_{\text{hom}} \exp\left(\frac{-\beta\vartheta^2\gamma_s^3}{k_b T \phi^2}\right) \tag{19}$$

where T is the temperature in degree Kelvin, k_b is the Boltzmann constant, and the pre-exponential expression (Ω_{hom}) can be written as in Eq. 20:

$$\Omega_{\text{hom}} = \frac{D}{d^5 N}\left(\frac{\Delta G_{\text{hom}}}{3\pi k_b T}\right)^{0.5} \tag{20}$$

where d is the inter-planer distance and D is the diffusion coefficient in the solution.

1.9. Heterogeneous nucleation in a solution

The presence of solid phase affect nucleation by decreasing the energy barrier of nucleation if the nucleus forms on the surface of the solid phase [1]. ΔG_{het} can be described in terms of homogeneous parameters, together with a single additional parameter $f(\theta)$ (Eq. 21–23), which represents the contact angle between the crystalline deposit and the solid substrate [18]:

$$\Delta G_{\text{het}} = f(\theta)\Delta G_{\text{hom}} \tag{21}$$

where

$$f(\theta) = \frac{(1-\cos\theta)(2+\cos\theta)}{4} \tag{22}$$

where θ represents the contact angle between the solid surface and the spherical nucleus [18].

The rate of heterogeneous nucleation can be evaluated from the change in Gibbs energy in a similar way to that used for homogeneous nucleation:

$$J = \Omega_{\text{het}} \exp\left(\frac{-\Delta G_{\text{het}}}{k_b T}\right) = \Omega_{\text{het}} \exp\left(\frac{-\beta\vartheta^2\gamma_S^3 f(\theta)}{k_b T \phi^2}\right) \tag{23}$$

where Ω_{het} is the pre-exponential expression for heterogeneous nucleation and $\Omega_{\text{het}} < \Omega_{\text{hom.}}$

In practice, the period of metastability preceding crystallization process is commonly indicated as the induction time (t_{ind}) [1,14,19,20]. The induction time calculation is inversely related to the nucleation rate as in Eqs. 24 and 25 [1]:

$$t_{\text{ind}} \alpha J^{-1} \tag{24}$$

where the nucleation steady state rate can be expressed as:

$$t_{\text{ind}} = \frac{1}{\Omega}\exp\left(\frac{\beta\vartheta^2\gamma_S^3 f(\theta)}{k_b T \phi^2}\right) \tag{25}$$

which can be written in a simplified way as follows:

$$\log t_{\text{ind}} = \frac{B}{(T)^3 \log^2 S_a} - A \tag{26}$$

where B and A are constants and can be expressed as in Eqs. 29 and 30:

$$B = \left[\frac{\beta\vartheta^2\gamma_S^3 f(\theta)}{v^2(2.3k_b)^3}\right] \tag{27}$$

and

$$A = \log \Omega \tag{28}$$

According to Sohnel and Mullin, 1982, if Log (t_{ind}) is plotted against $T^{-3}\text{Log}^{-2}\ S_a$ for a wide range of saturations, two slopes can be identified where each represents a particular nucleation mechanism [19]. The steeper slope represents the homogenous zone of nucleation while the lower slope represents the heterogeneous one. In between the two slopes is an intermediate zone where a smooth transition between the two nucleation mechanisms may takes place.

Experimentally the measured induction time may also include growth to a detectable size [1].The induction time in such case is proportional to both nucleation (J) and growth rates (G) as shown in Eq. 29 [21–23]:

$$t_{\text{ind}}\alpha(G^3J)^{-\frac{1}{4}} \tag{29}$$

For a limited range of supersaturation and constant temperature, no change in the nucleation mechanism is expected and the relation can be written as a linear fit between the logarithm of the induction time and that of the saturation ratio (Eq. 30) [1,24–26]:

$$\log t_{\text{ind}} = k - n\log(S_a) \tag{30}$$

where k is a constant with no physical meaning and n is the order.

1.10. $CaCO_3$ phases

According to Eq. 30 the induction time depends strongly on the saturation (S_a). The seawater saturation is known to be affected by the ionic strength, affecting the solubility of $CaCO_3$ and acidity constants. High ionic strength increases the CO_2 solubility as well as the acidic constants leading to, if not taken into consideration, an overestimation of the saturation [27–35]. Some researchers have claimed the formation of other forms of $CaCO_3$ other than calcite [1,12,28,29,36–39].

Ostwald's rule of stage (1897) states that an unstable system does not necessarily transform directly into the most stable state, but may be preceded by one which most closely resembles its own, i.e., into another transient stage which possesses greater energy than that of the stable phase [1,40].

Based on Ostwald's rule of stage, the activation energy for the formation of $CaCO_3$ must exceed that of the least stable form. In this specific case and depending on temperature, the first precipitating phase will be either amorphous calcium carbonate (>30°C) or ikaite ($CaCO_3\ 6H_2O$) (<25°C) or amorphous and monohydrated depending on the mechanism of nucleation as amorphous $CaCO_3$ (100 times higher in solubility than calcite) formation is associated with homogenous nucleation and monohydrated $CaCO_3$ (40 times higher than calcite) with heterogeneous nucleation [36,39,41].

By the formation of the first precipitating phase, the reaction continues until the formation of calcite which is the most stable form of $CaCO_3$. This was explained by the kinetics of transformation, which means that the phase which has the highest formation rate is more likely to form (e.g., monohydrated $CaCO_3$ to vaterite) than that which has more favourable thermodynamics (e.g., monohydrated to calcte) [1,42].

Calcite as the most stable form of $CaCO_3$ has been extensively studied by different researchers [1,27,43]. Other compounds such as aragonite, vaterite, amorphous, monohydrated and hexahydrated calcium carbonate have been studied less. The solubility of different $CaCO_3$ species is temperature-dependent [12]. Normally the solubility of $CaCO_3$ species decreases with temperature except for the hexahydrated form.

2. Materials

2.1 pH meter

The induction time measurements using pH were performed by a highly sensitive pH meter (Eutech pH 6000) with an accuracy of 0.001 pH units. pH can be measured online using the manufacturer's (Eutech) software or offline by using the instrument memory for sample storage. The measuring interval can be adjusted to as low as every 30 s.

2.2. Reactors

The pH probe was fitted in the top of the air-tight double-jacketed glass reactor (Applikon) with a volume of 3 l, and equipped with a double-paddled shaft mechanical stirrer. The mixing rate can be varied from 0 to 1200 rpm using an electronic controller (Applikon) linked to the motor of the mixer. The reactor can be filled either manually or mechanically using a diaphragm pump with an average filling speed of 4 l/min.

After each experiment, cleaning was employed with 0.2 molar HNO_3 for 30 min with a flow of 0.15 l/min to dissolve any formed crystals. The reactor was then flushed with de-mineralized water for 15 min with a flow rate of 3 l/min before the next experiment.

2.3. Synthetic seawater concentrate preparation

The preparation of ultra-pure water starts by delivering tap water as the raw water source where it passes through a series of treatment steps to decrease the organic and inorganic particle content in the feed water. The product water had a conductivity and total organic carbon (TOC) of 0.8 µS/cm and 3 µg/l, respectively. The TOC was measured using a TOC analyzer with a detection limit of 0.5 µg/l.

Table 2
Salt reagents used in the experimental synthetic seawater concentrate preparation

Reagent	Form	Supplier	Purity
NaCl	Salt	J.T. Baker	99.5–99.9%
$CaCl_2$ $2H_2O$	Salt	MERCK	99.9
$NaHCO_3$	Salt	MERCK	99.9

The synthetic seawater concentrate used in the experiments are prepared in stages. Firstly, $NaHCO_3$ solution was prepared by dissolving $NaHCO_3$ salt (Table 2) in ultrapure water. Secondly, a $CaCl_2$. solution was prepared by dissolving $CaCl_2$ $2H_2O$. Finally, NaCl salt was dissolved in the previously prepared $CaCl_2$ $2H_2O$ solution to adjust the salinity values of the prepared synthetic concentrate to the desired levels.

To ensure a complete dissolution of the reagents, the preparation step involves dissolving the solutions on a 1 l batch basis. The salt was added to the ultra-pure water in a measuring flask. The flask was then closed and shaken manually for 2 min after which 2 h of solution mixing took place on a magnetic stirrer. Mixing was performed at an average speed of 400 rpm and at a room temperature of 20°C.

The induction time experiments were initiated by adding the $NaHCO_3$ solution into the reactor followed by the addition of 0.2 M NaOH solution for pH correction (if needed). The mixing rate during addition is kept at 150 rpm to prevent the formation of local areas with higher saturation than desired one. Finally the $CaCl_2$. + NaCl solution was added with a rate of 0.2 l/min while maintaining same mixing rate. The addition was performed through fine nozzles located 3 cm from the reactor's base accompanied by vigorous mixing to ensure proper distribution of the solution when added. The two reacting solutions were added on a 1:1 volume basis.

3. Methods

3.1. Induction time measurements

The pH change was monitored over a period of 1000 min, and the induction time was defined as a pH decrease of at least 0.03 pH units. This decrease is equivalent to less than 0.1–0.27 mg/l of precipitated $CaCO_3$ (30–50 times lower than the total precipitated) depending on the added HCO_3^- concentration which is constant for each ionic strength tested but fixed for each recovery. The mixing rate was kept constant at 150 rpm using an electronic controller linked to the mixing motor and the start of the experiment was defined as the time of complete addition of the reacting solutions. Experimental temperature was kept constant at 20 and 25°C using temperature controller.

3.2. Solutions concentrations

Four experimental matrixes were used in the induction time experiments with ionic strengths of I = 0.054, 1.12, 1.34, 1.61 mole/l (Table 3). For the lower ionic strength range the Ca^{2+} and the HCO_3^- content were 667 and 209 mg/l, respectively. In the higher range these amounts were increased to 948 and 293 mg/l, respectively. These amounts of Ca^{2+} and HCO_3^- are equivalent to those found in SWRO concentrates using Gulf of Oman water at recovery rates of 30% and 50% (Table 1).

3.3. Calculation of SI using PhreeqC

The Phreeqc program was used to calculate the activity product by incorporating the activity coefficient to account for the ionic complexation due to the increase in salinity. The SI calculations in this study used the ionic activity product from Phreeqc and equations presented in Table 2 for the calculation of different $CaCO_3$ phase saturations.

4. Results

Table 4 represents the results for the experimental data between the initial pH, initial SI and induction time at four different ionic strength values of I = 0.054, 1.12, 1.34 and 1.61 mole/l (Table 4).

The relation between Log t_{ind} and Log (S_a) represented in Fig. 1 showed a correlation factor ranging between 0.93–0.95 when Eq. 32 describing the nucleation mechanism for a limited range of saturation was used.

Adopting the same concept, the relation between S&DSI and the logarithm of the induction time (Fig. 2) was plotted. The results showed two different zones than that found in Fig. 1 between SI and the logarithm of the induction time. In Fig. 2 the first zone contains the low ionic strength induction time experiments (I = 0.054 mole/l) while the second contains the higher ionic strength experiments (I = 1.12, 1.34, 1.61 mole/l). In the first zone (I = 0.054), the S&DSI values were nearly 0.5–1.1 units of magnitude less if compared to the S&DSI values obtained at the same induction time values at high ionic strength solutions (I = 1.12, 1.34, 1.61 and represented in Table 4).

Table 3
The experimental solution's ionic strength and the corresponding calcium and bi-carbonate content

Recovery	%	30%		50%	
Ionic strength	Mole/l	0.054	1.12	1.34	1.61
Ca^{2+}	mg/l	677	677	948	948
HCO_3^-	mg/l	209	209	293	293
Na^+	mg/l	79	29829	35410	42890
Cl^-	mg/l	1182	30932	36980	44460

Table 4
The induction time experimental results at different ionic strength for synthetic seawater concentrates

I mole/l	Initial pH	t_{ind} (min)	Log t_{ind}	Initial S&DSI	T^{o}K	Initial SI (calcite)
0.054	7.84	173	2.24	1.20	298	1.31
	7.83	192	2.28	1.19	298	1.30
	8.12	41	1.61	1.48	298	1.57
	8.26	37	1.57	1.62	298	1.68
	8.28	23	1.36	1.64	298	1.69
	8.4	22	1.34	1.76	298	1.79
	8.41	17	1.23	1.77	298	1.80
	8.56	15	1.18	1.92	298	1.91
	8.58	11	1.04	1.94	298	1.92
	8.81	11	1.04	2.17	298	2.03
	8.75	5	0.70	2.11	298	2.07
1.12	7.82	678	2.83	0.03	293	0.81
	8.04	374	2.57	0.25	293	1.02
	8.28	184	2.26	0.49	293	1.23
	8.32	240	2.38	0.53	293	1.26
	8.42	114	2.06	0.63	293	1.35
	8.50	138	2.14	0.71	293	1.41
	8.63	100	2.00	0.84	293	1.51
	8.68	73	1.86	0.89	293	1.54
	8.79	41	1.61	1.00	293	1.61
	8.88	25	1.40	1.09	293	1.67
	8.98	26	1.41	1.19	293	1.73
	9.04	40	1.60	1.25	293	1.76
	9.10	22	1.34	1.31	293	1.79
1.34	7.93	114	2.06	0.54	298	1.29
	8.23	60	1.78	0.84	298	1.55
	8.33	49	1.69	0.94	298	1.63
	8.42	48	1.68	1.03	298	1.69
	8.52	21	1.32	1.13	298	1.77
	8.62	22	1.34	1.23	298	1.83
	8.79	17	1.23	1.40	298	1.93
1.61	7.51	778	2.89	0.07	293	0.87
	7.56	554	2.74	0.12	293	0.91
	7.82	168	2.23	0.38	293	1.16
	7.83	181	2.26	0.39	293	1.17
	7.91	101	2.00	0.47	293	1.24
	7.92	114	2.06	0.48	293	1.25
	8.00	85	1.93	0.56	293	1.29
	8.04	62	1.79	0.60	293	1.35
	8.09	49	1.69	0.65	293	1.40
	8.09	60	1.78	0.65	293	1.40
	8.20	55	1.74	0.76	293	1.49
	8.20	44	1.64	0.76	293	1.49

Continued

Table 4 *Continued*

I mole/l	Initial pH	t_{ind} (min)	Log t_{ind}	Initial S&DSI	T°K	Initial SI (calcite)
	8.23	41	1.61	0.79	293	1.52
	8.25	28	1.45	0.81	293	1.53
	8.25	24	1.38	0.81	293	1.53
	8.27	20	1.30	0.83	293	1.55
	8.31	21	1.32	0.87	293	1.58
	8.34	19	1.28	0.90	293	1.60
	8.41	20	1.30	0.97	293	1.66
	8.41	22	1.34	0.97	293	1.66
	8.43	9	0.95	0.99	293	1.67
	8.43	14	1.15	0.99	293	1.68
	8.52	11	1.04	1.08	293	1.74
	8.52	18	1.26	1.08	293	1.74
	8.53	13	1.11	1.09	293	1.74
	8.54	10	1.00	1.10	293	1.75
	8.60	13	1.11	1.16	293	1.79
	8.62	7	0.85	1.18	293	1.80
	8.64	4	0.60	1.20	293	1.82
	8.67	7	0.85	1.23	293	1.84

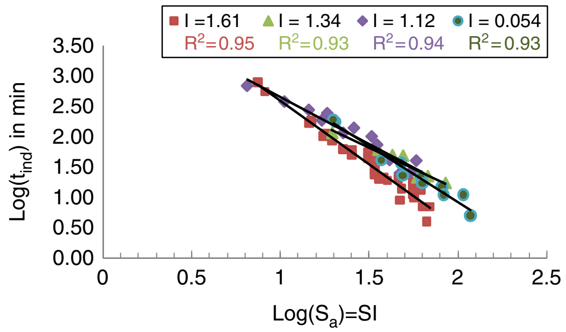

Fig. 1. Log t_{ind} vs. Log (S_a) for I = 0.054 and 1.34 mole/l at 25°C and for I = 1.12 and 1.61 mole/l at 20°C.

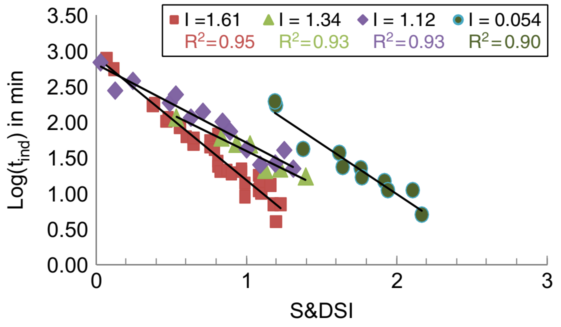

Fig. 2. Comparison relationship between Log t_{ind} vs. S&DSI for I = 0.054 and 1.34 mole/l at 25°C and for I = 1.12 and 1.61 mole/l at 20°C.

Results in Table 4, Figs. 1 and 2 shows that the value of the SI and S&DSI at low ionic strength solutions are comparable. On the contrary, at higher ionic strength solutions values the S&DSI values were nearly 0.5 units of magnitude less compared to that of SI. A possible explanation is that the S&DSI and SI are using similar solubility product value (calcite in such case) but different solubility product value at high ionic strength but this hypothesis needs to be further investigated.

4.1. The Solubility product used by the S&DSI

A relation between SI, S&DSI and pH was established for different $CaCO_3$ phases to determine the K_{sp} value incorporated in the S&DSI (Figs. 3–6). In Figs. 3, 4, 5 for I = 1.61, 1.34, 1.12 mole/l, the results suggest that to have the SI and the S&DSI value are comparable if the solubility of vaterite is used in the SI calculation. On the other hand, at the lower ionic strength of I = 0.054 (Fig. 6), the SI and the S&DSI values were nearly equal when the K_{sp} was in the range of calcite. It is worth mentioning that the change in the phase solubility used by Stiff & Davis, 1952 may be attributed to their experimental procedure which depend on shaking the supersaturated solution and measuring the solubility after 24 h at different ranges of ionic strength [9].

Samples were taken after 24 h from the reactor at the end of the induction experiments for solutions with I = 0.054 and analyzed in wet conditions under an

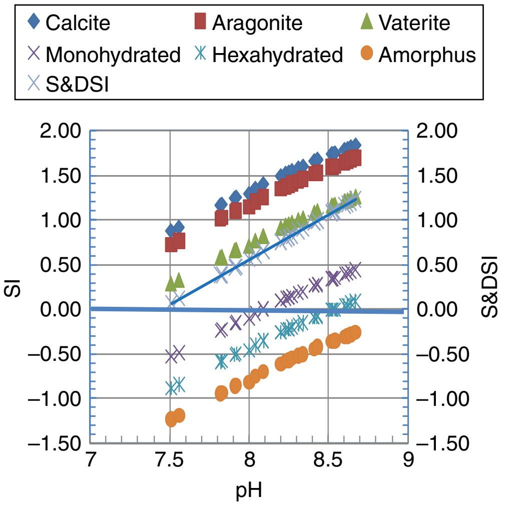

Fig. 3. Comparison relationship between SI and S&DSI (crosses with blue line) vs. pH for different phases at $I = 1.61$.

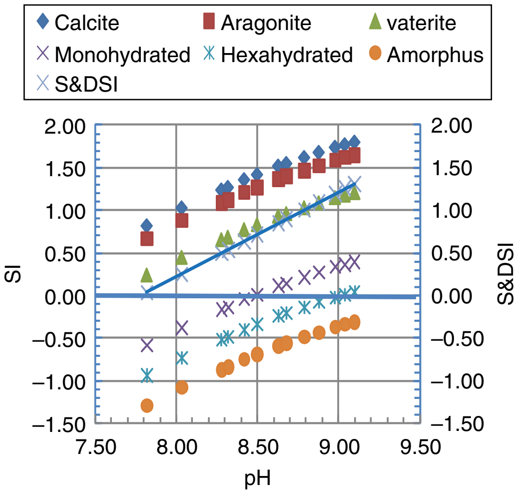

Fig. 5. Comparison relationship between SI and S&DSI (crosses with blue line) vs. pH for different phases at $I = 1.12$.

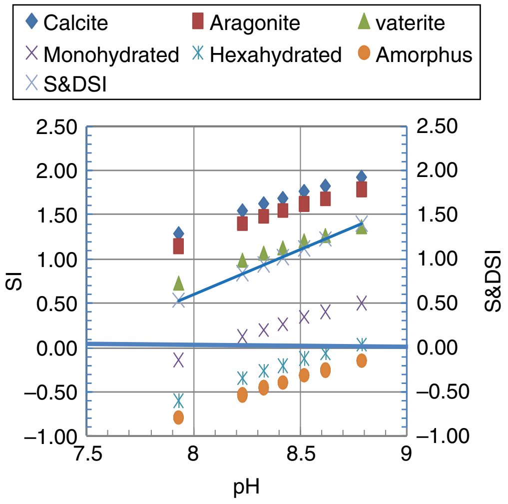

Fig. 4. Comparison relationship between SI and S&DSI (crosses with blue line) vs. pH for different phases at $I = 1.34$.

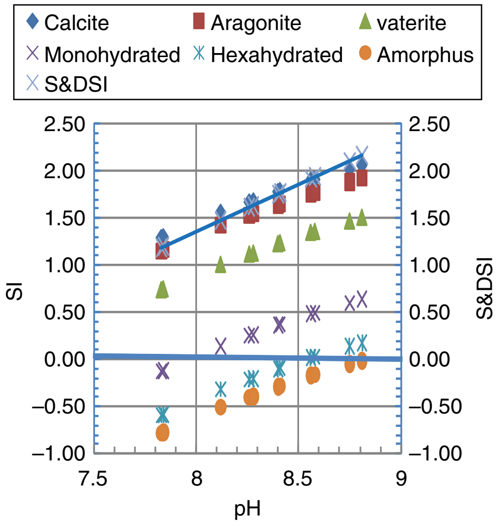

Fig. 6. Comparison relationship between SI and S&DSI (crosses with blue line) vs. pH for different phases at $I = 0.054$.

electron microscope (Fig. 7). Results showed a mixture of vaterite (hexagonal shape) and calcite (rhombus) crystals. These findings were very similar to those found by Clarkson et al. 1997 where a mixture of vaterite and calcite was found as an end product of their nucleation experiments [44]. The same was reported when vaterite is abundant at seawater temperatures from 20–50°C and transformed into calcite due to its instability [45]. The presence of vaterite at the end of the experiment suggests that SI calculated using the K_{sp} of calcite and S&DSI calculations for low ionic strength solutions are overestimating the supersaturation by a factor of 0.5 compared to that calculated using calcite solubility. At high ionic strength solutions, vaterite could be considered and not calcite in the calculations of SI as the K_{sp} of vaterite is found to be the most probable phase incorporated in the S&DSI.

4.2. Homogenous and heterogeneous nucleation

Comparing our research data against the data of Sohnel and Mullin 1982 (Fig. 8); the same pattern was found [19]. The results show that for low ionic strength experiment ($I = 0.054$) nearly all the results lies in the homogenous zone identified by Sohnel and Mullin, 1982 while data points for high ionic strength solutions

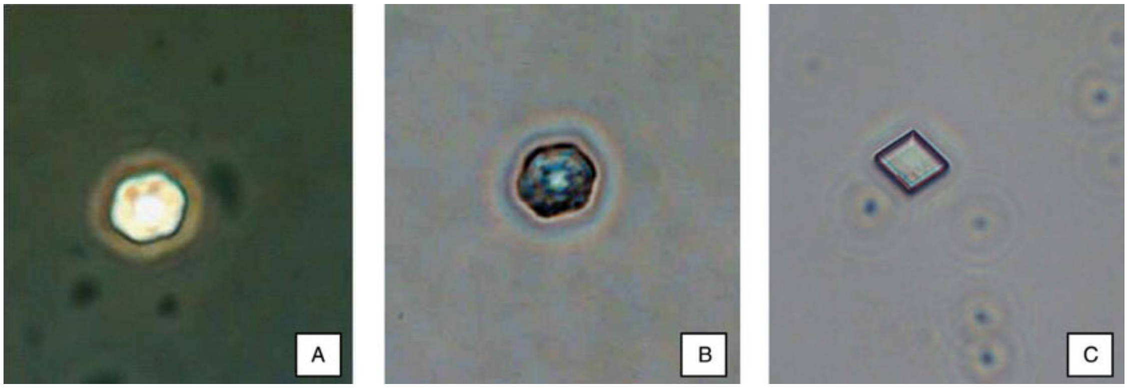

Fig. 7. Water ($I = 0.054$) and the solution saturation S_a of 42 at 25°C, A and B- the vaterite hexagonal crystal C- calcite crystal shape.

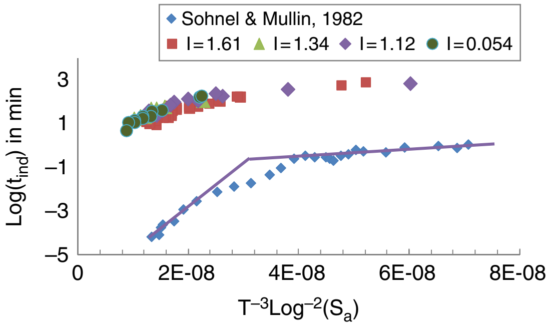

Fig. 8. Induction time results of this research compared to Sohnel and Mullin, 1982 data for the classification of homogenous and heterogeneous mechanism.

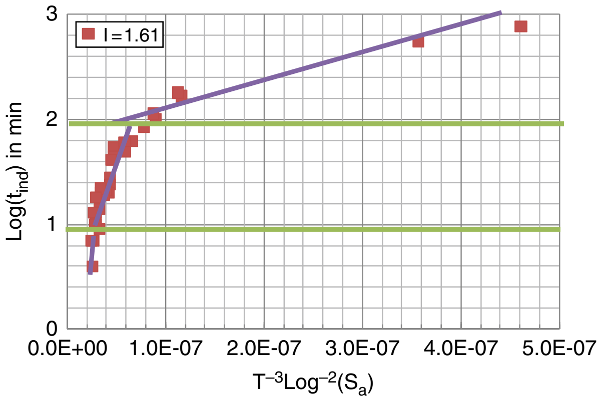

Fig. 9. Nucleation zones for solution with I = 1.61 based on the classification adopted from Sohnel and Mullin, 1982 [19].

(I = 1.12, 1.34 and 1.61) covered both the homogenous and heterogeneous nucleation zones [19].

Fig. 9 and Table 5 represents the relation between log (t_{ind}) and $T^{-3}\mathrm{Log}^{-2}\ S_a$ in a synthetic solution of I=1.61 mole/l. The results show three identified zones representing the homogenous nucleation, the heterogeneous nucleation and an intermediate zone with different slope 3E+6, 2E+7 and 8E+8 (Table 7) and similar to those identified by Sohnel and Mullin, 1982 [19]. The first cover values of $T^{-3}.\mathrm{Log}^{-2}(S_a)$ of less than 1.25×10^{-8} and the second covers the zone from 1.25×10^{-8} to 2.0×10^{-8} while the third covers the range values higher than 2.6×10^{-8}. As each line covers a limited range of supersaturation, it can be considered to represent a different nucleation surface energy (different $\gamma_s^3 f(\theta)$) [1]. The steeper line represents the homogenous nucleation zone while the line with the lower slope represents the heterogeneous one.

Fig. 10 shows the initial SI using different K_{sp} values for hydrated and unhydrated $CaCO_3$ phases as a function of log (t_{ind}). Fig. 10 and Table 5 was divided into three zones based on the initial saturation compared to the $CaCO_3$ phases. At the first zone (Log t_{ind} <1.1) the experimental solution was initially supersaturated with respect to the unhydrated phases (calcite, aragonite, vaterite) but not to the hydrated phases (amorphous, hexahydrated, monohydrated). In the second zone (1.79 <Log t_{ind} >1.1), the solution was supersaturated with regard to monohydrated $CaCO_3$ but undersaturated with respect to hexahydrated and amorphous $CaCO_3$. In the third zone (Log t_{ind} >1.79), the solution was supersaturated with hexahydrated $CaCO_3$ but not with amorphous $CaCO_3$. In this identified third zone, the increase in the initial pH (>8.53) of the solution in order to increase SI hardly increases the solution saturation and therefore, amorphous $CaCO_3$ saturation could not be reached in our experiments.

The borders of the three identified zones are identical to the points of slope change in Fig. 9 and Table 5 and hence the mechanism of nucleation. The results suggest that homogeneous nucleation predominates only when

Table 5
Nucleation mechanism classification based on $I = 1.61$ mole/l

	pH	t_{ind} (min)	Log t_{ind}	$T^{-3}.\text{Log}^{-2}(S_a)$	K_{sp}					
					8.45 Calcite	8.31 Aragonite	7.87 Vaterite	7.05 Mono-hydrated	6.70 Hexa-hydrated	6.35 Amorphous
					SI					
Group 1	7.51	778	2.89	5.2E−08	0.87	0.73	0.29	−0.53	−0.88	−1.23
Heterogeneous	7.56	554	2.74	4.8E−08	0.91	0.77	0.33	−0.49	−0.84	−1.19
	7.82	168	2.23	2.9E−08	1.16	1.02	0.58	−0.24	−0.59	−0.94
	7.83	181	2.26	2.9E−08	1.17	1.03	0.59	−0.23	−0.58	−0.93
	7.91	101	2.00	2.6E−08	1.24	1.10	0.66	−0.16	−0.51	−0.86
	7.92	114	2.06	2.5E−08	1.25	1.11	0.67	−0.15	−0.50	−0.85
	8.00	85	1.93	2.4E−08	1.29	1.15	0.71	−0.11	−0.46	−0.81
	8.04	62	1.79	2.2E−08	1.35	1.21	0.77	−0.05	−0.40	−0.75
Group 2	8.09	60	1.78	2.0E−08	1.40	1.26	0.82	0.00	−0.35	−0.70
Intermediate	8.09	49	1.69	2.0E−08	1.40	1.26	0.82	0.00	−0.35	−0.70
	8.20	55	1.74	1.8E−08	1.49	1.35	0.91	0.09	−0.26	−0.61
	8.20	44	1.64	1.8E−08	1.49	1.35	0.91	0.09	−0.26	−0.61
	8.23	41	1.61	1.7E−08	1.52	1.38	0.94	0.12	−0.23	−0.58
	8.25	28	1.45	1.7E−08	1.53	1.39	0.95	0.13	−0.22	−0.57
	8.25	24	1.38	1.7E−08	1.53	1.39	0.95	0.13	−0.22	−0.57
	8.27	20	1.30	1.6E−08	1.55	1.41	0.97	0.15	−0.20	−0.55
	8.31	21	1.32	1.6E−08	1.58	1.44	1.00	0.18	−0.17	−0.52
	8.34	19	1.28	1.5E−08	1.60	1.46	1.02	0.20	−0.15	−0.50
	8.41	20	1.30	1.4E−08	1.66	1.52	1.08	0.26	−0.09	−0.44
	8.41	22	1.34	1.4E−08	1.66	1.52	1.08	0.26	−0.09	−0.44
	8.43	14	1.15	1.41E−08	1.68	1.54	1.10	0.28	−0.07	−0.42
	8.43	9	0.95	1.4E−08	1.67	1.53	1.09	0.27	−0.08	−0.43
	8.52	11	1.04	1.3E−08	1.74	1.60	1.16	0.34	−0.01	−0.36
	8.52	18	1.26	1.3E−08	1.74	1.60	1.16	0.34	−0.01	−0.36
	8.53	13	1.11	1.3E−08	1.74	1.60	1.16	0.34	−0.01	−0.36
Group 3	8.54	10	1.00	1.3E−08	1.75	1.61	1.17	0.35	0.00	−0.35
Homogenous	8.60	13	1.11	1.2E−08	1.79	1.65	1.21	0.39	0.04	−0.31
	8.62	7	0.85	1.2E−08	1.80	1.66	1.22	0.40	0.05	−0.30
	8.64	4	0.60	1.2E−08	1.82	1.68	1.24	0.42	0.07	−0.28
	8.67	7	0.85	1.2E−08	1.84	1.70	1.26	0.44	0.09	−0.26

the initial solution saturation exceeds that of hexahydrated $CaCO_3$. The intermediate zone, exists when the initial saturation in the range between monohydrated $CaCO_3$ and hexahydrated $CaCO_3$. In the lower saturation range (lower than monohydrated $CaCO_3$) heterogeneous nucleation predominates. Therefore these results may suggest that the mechanism of nucleation is related not only to the solution saturation but must also be combined with the phase of the $CaCO_3$.

Accordingly, following the same procedure, Figs. 11 and 12 were drawn for a synthetic solution with $I = 1.12$ using the experimental results represented in Table 6. The concept appears to be valid in the heterogeneous zone where the solution is supersaturated with respect

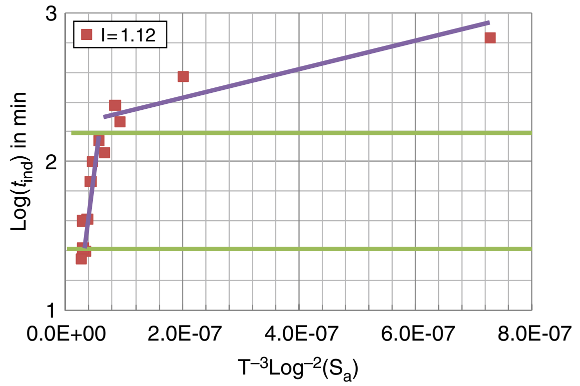

Fig. 11. Nucleation zones for solution with $I = 1.12$ based on the classification adopted after Sohnel and Mullin, 1982 [19].

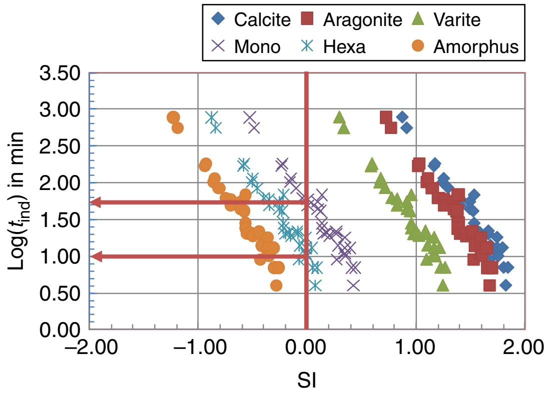

Fig. 10. Relation between the log (t_{ind}) and the SI using the solubility of different phases of $CaCO_3$ for solution with $I = 1.61$ mole/l.

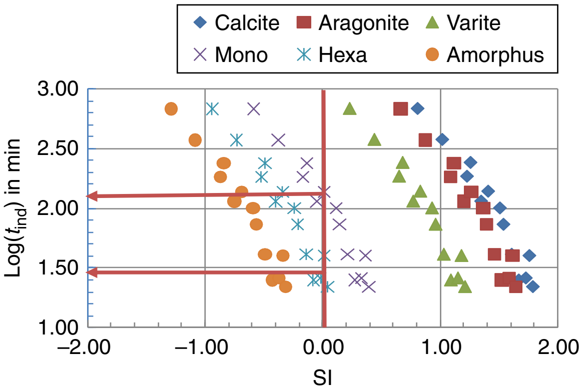

Fig. 12. Relation between the log (t_{ind}) and the SI using the solubility of different phases of $CaCO_3$ for solution with $I = 1.12$ mole/l.

Table 6
The nucleation mechanism classification based on $I = 1.12$ mole/l

	pH	t_{ind} (min)	Log t_{ind}	T^{-3}.Log^{-2} (S_a)	K_{sp}					
					8.45 Calcite	8.31 Aragonite	7.87 Vaterite	7.05 Mono-hydrated	6.70 Hexa-hydrated	6.35 Amorphous
Group 1	7.82	678	2.83	6.0E−08	0.81	0.67	0.23	−0.59	−0.94	−1.29
	8.04	374	2.57	3.8E−08	1.02	0.88	0.44	−0.38	−0.73	−1.08
	8.28	184	2.26	2.6E−08	1.23	1.09	0.65	−0.17	−0.52	−0.87
	8.32	240	2.38	2.5E−08	1.26	1.12	0.68	−0.14	−0.49	−0.84
	8.42	114	2.06	2.2E−08	1.35	1.21	0.77	−0.05	−0.40	−0.75
Group 2	8.50	138	2.14	2.0E−08	1.41	1.27	0.83	0.01	−0.34	−0.69
	8.63	100	2.00	1.7E−08	1.51	1.37	0.93	0.11	−0.24	−0.59
	8.68	73	1.86	1.7E−08	1.54	1.40	0.96	0.14	−0.21	−0.56
	8.79	41	1.61	1.5E−08	1.61	1.47	1.03	0.21	−0.14	−0.49
	8.88	25	1.40	1.4E−08	1.67	1.53	1.09	0.27	−0.08	−0.43
	8.98	26	1.41	1.3E−08	1.73	1.59	1.15	0.33	−0.02	−0.37
Group 3	9.04	40	1.60	1.3E−08	1.76	1.62	1.18	0.36	0.01	−0.34
	9.10	22	1.34	1.2E−08	1.79	1.65	1.21	0.39	0.04	−0.31

Table 7
The intersection and slope values (*A* and *B*) in Eqs. 28, 29 and 30 for the three identified nucleation mechanism zones for solution of *I* = 1.61

Ionic strength	*I* = 1.61	*A*	*B*
I = 1.61	Heterogeneous nucleation zone	–1.7346	3.00E+06
	Intermediate nucleation zone	–0.3806	2.00E+07
	Homogenous nucleation zone	+1.1132	8.00E+08
I = 0.054	Heterogeneous nucleation zone	—	—
	Intermediate nucleation zone	-0.6011	3.00E+07
	Homogenous nucleation zone	+0.475	8.00E+07

Table 8
The calculations of the apparent surface energy using Eq. 27

I mole/l	*B*	k_a	k_v	β	ρ	*m*	υ	θ	$\gamma_s^3 f(\theta)$	γ_s *(apparent)* mJ/m^2
1.61	3.00E+06	1	6	32	2660	0.1	2	6.24E–29	3.08E–06	15
	2.00E+07	1	6	32	2660	0.1	2	6.24E–29	2.05E–05	27
	8.00E+08	1	6	32	2660	0.1	2	6.24E–29	8.21E–04	94
0.054	0.00E+00	1	6	32	2660	0.1	2	6.24E–29	0.00E+00	0.0
	3.00E+07	1	6	32	2660	0.1	2	6.24E–29	3.08E–05	31
	8.00E+07	1	6	32	2660	0.1	2	6.24E–29	8.21E–05	43

to the unhydrated phases but undersaturated with the hydrated ones. When the monohydrated saturation was surpassed, a different slope (9E+7) was found representing the same transitional period as the one found earlier in Figs. 9 and 10. The final stage of homogenous nucleation was not identified in this figure due to the lack of data (there were only two measurement points).

In order to determine the effect of the mechanism of nucleation on the surface energy of the nuclei formed, the slopes of the lines found in Figs. 9 and 11 were calculated and represented in Table 7. The slope (*B*) represented in Eq. (27) was used to calculate the surface energy.

The results represented in Table 8 show the calculations of the surface energy based on the classical nucleation theory for vaterite. The surface energy values obtained were in the range of 15–94 mJ/m^2. These values are consistent with literature values for vaterite when the heterogeneous nucleation mechanism predominates except for the higher value of 94 mJ/m^2 which is consistent with theoretical literature values of (90-141 mJ/m^2) for surface energy of vaterite when homogenous nucleation mechanism predominates [41,43,46–54]. It is worth mentioning that the uncertainty in the shape factor (β) of the blocks building the formed nuclei (either spheres or cubes) will affect the resultant surface energy value e.g. using the shape factor for spheres instead of cubes will result in a surface energy value of 114 mJ/m^2 instead of 94 mJ/m^2. Furthermore, the value of surface energy was reported to be affected by the experimental technique used where the free drift method (similar to what is used in this work) normally results in a much lower surface energy value compared to the constant composition method [48,52,53].

5. Conclusions

1. For high ionic strength waters (>1.1.2), results suggested that S&DSI incorporates vaterite solubility in its calculation.
2. The results suggested that vaterite is most likely the precipitating phase and not calcite. Incorporating the solubility of vaterite and not calcite in the SI calculation will result in a decrease in SI by about 0.5 units compared to that using the solubility of calcite.
3. The relation between log t_{ind} and $T^{-3}\mathrm{Log}^{-2}(S_a)$ can be used to identify the nucleation mechanism of $CaCO_3$. For *I* = 1.12 and 1.61 mole/l, three different slopes were found where the steepest slope represents the

homogenous nucleation and the shallower line representing the heterogeneous nucleation zone. An intermediate zone with different line slope and consequently a different surface energy was recognized.

4. The nucleation mechanism involved in the induction time experiment is closely related to the initial synthetic solution saturation. A homogenous precipitation appears to predominate when the initial solution saturation exceeded that of hexahydrated $CaCO_3$ (ikaite) and the heterogeneous nucleation appears to predominate when the initial saturation is less than the monohydrated but higher than vaterite. In between, an intermediate zone where the initial saturation is below the ikaite but higher than the hexahydrated.
5. The surface energy calculations using the classical nucleation theory result in surface energy values of 15–94 mJ/m^2 which is consistent with values in literature for spontaneous precipitation of $CaCO_3$.

Symbols

A — Function of Pre-exponential factor (s^{-1}/m^3)
A^* — Deby Huckel constant (L$^{2/3}$/mole$^{1/2}$)
A_N — Nuclei surface area (m^2)
a_c — Activity
A_f — Free area for precipitation at given particle size (m^2)
Alk — Alkalinity of solution (mole/l)
B — Constant expressed (L$^{3/2}$mole^{-1}/m)
D — Diffusion coefficient in the solution
d — Interplaner distance in solid phase (m)
ΔG_{hom} — The change in Gibbs energy in the homogenous zone (J)
ΔG_{het} — The change in Gibbs energy in the heterogeneous zone (J)
G — Growth rate (mole/min/cm^3)
I — The ionic strength (mole/l)
J — Nucleation rate (nuclei/min/cm^3)
K_a — Area geometric factor
K_{a2} — Temperature corrected second acidity constant (mole/l)
k_b — Boltzmann constant (J/K)
K_{so} — Solubility at standard conditions (mole^2/l^2)
K_{sp} — Solubility product (mole^2/l^2)
K — Graphical obtained constant in S&DSI calculations
k_a — Area geometric factor
k_v — Volume geometric factor
Log — Log_{10}
N — Number of molecules
n — the order of nucleation
P — Pressure (psi)
pAlk — Negative the logarithm of alkalinity activity divided by its dimensions
pCa — Negative the logarithm of calcium activity divided by its dimensions
pH — Concentrate pH
pH_s — Equilibrium pH
S_a — Supersaturation ratio
SI — Supersaturation Index
r — Nuclei radius (m)
r^* — Critical nuclei radius (m)
T — Absolute temperature (Kelvin)
t_{ind} — Induction time in minutes unless mentioned otherwise (min)
V — The nuclei volume
υ — Number of ions into which a molecule dissociates
X — A constant with no physical meaning

Greek letters

$f(\theta)$ — Factor differentiating heterogeneous and homogenous nucleation
β — Geometric factor
θ — Molecular volume (cm^3/mole)
$\gamma+$ — Cation activity coefficient
γ_- — Anion activity coefficient
γ_s — Surface energy (J/m^2)
Ω — Pre-exponential factor in the nucleation rate equation (s^{-1}/m^3)
δ — Pre-exponential factor in the nucleation rate equation

References

[1] O. Sohnel and J. Garside, Precipitation basis principals and industrial applications, 1992, Oxford: Butterworth-Heinemann.
[2] J. Butler, Ionic Equilibrium: Solubility and pH calculations, 1998, New York: John Wiley & Sons.
[3] S. Boerlage, et al., Stable barium sulphate supersaturation in reverse osmosis, J. Membr. Sci., 179 (2000) 53–68.
[4] S. Boerlage, et al., $BaSO_4$ solubility in reverse osmosis concentrates, J. Membr. Sci., 159 (1999) 47–59.
[5] E. Kirkova and M. Djarova, On the Kinetics of Crystallization of Zinc Oxalate Dihydrate by Precipitation Industrial Crystallization, 78 (1979) 81–89.
[6] S. Patel and M. Finan, New antifoulants for deposit control in MSF and MED plants, Desalination, 124 (1999) 63–74.
[7] S. Lee, J.S. Choi and Z.H. Lee, Behaviors of dissolved organic matter in membrane desalination, Desalination, 238 (2009) 109–116.
[8] ASTM-D4582-91, Calculation and Adjustment of the Stiff and Davis Stability Index for Reverse Osmosis, 2001, ASTM International: West Conshohocken, PA, United States.
[9] H.A. Stiff and L.E. Davis, A method for predicting the tendency of oil field waters to deposit calcium carbonate, Petroleum transactions, 195 (1952) 213–216.
[10] R. Sheikholeslami, Mixed salts—scaling limits and propensity, Desalination, 154(2) (2003) 117–127.
[11] K.S. Pitzer and G. Mayorga, Thermodynamics of electrolytes (III) Activity and osmotic coefficients for 2-2 electrolytes, J. Soln. Chem., 3 (1973) 539–546.
[12] H. Elfil and H. Roques, Kinetics of the precipitation of calcium sulfate dihydrate in a desalination unit, Desalination, 157 (2003) 9–16.

[13] L.A. Bromley, Thermodynamic properties of strong electrolytes, AIChE J., 19(2) (1973) 313–320.
[14] S. Boerlage, Scaling and particulate fouling in membrane filtration system, in Sanitary Engineering, 2002, IHE: Delft.
[15] Y. Wang, Composite fouling of calcium sulphate and calcium carbonate in a dynamic seawater reverse osmosis unit, 2005, University of New South Wales: Sydney.
[16] E. Darton, Membrane chemical research: centuries apart, Desalination, 132 (2000) 121–131.
[17] V. Snoeyink and D. Jenkins, Water Chemistry, 1980, New York: John Wiley & Sons, Inc.
[18] Y. Liu and G.H. Nancollas, Fluorapatite growth kinetics and the influence of solution composition, J. Cryst. Growth, 165(1–2) (1996) 116–123.
[19] O. Sohnel and J.W. Mullin, Precipitation of calcium carbonate, J. Cryst. Growth, 60 (1982) 239–250.
[20] O. Sohnel and J.W. Mullin, Influence of mixing on batch precipitation Crystal Research and Technology, 22(10) (1987) 1235–1240.
[21] M. Avrami, Kinetics of phase change: I general theory, J. Chem. Phys., 7(12) (1939) 1103–1112.
[22] M. Avrami, Kinetics of phase change: II transformation time relations for random distribution of nuclei. J. Chem. Phys., 8(2) (1940) 212–224.
[23] M. Avrami, Kinetics of phase change: III granulation, phase change, and microstructure, J. Chem. Phys., 9(2) (1941) 177–184.
[24] S.V. Golubev, O.S. Pokrovsky and V.S. Savenko, Unseeded precipitation of calcium and magnesium phosphates from modified seawater solutions, J. Cryst. Growth, 205 (1999) 354–360.
[25] V. Sergei, O.S. Pokrovsky and V.S. Savenko, Unseeded precipitation of calcium and magnesium phosphates from modified seawater solutions, J. Cryst. Growth, 205 (1999) 354–360.
[26] S.V. Golubev, O.S. Pokrovsky and V.S. Savenko, Homogeneous precipitation of magnesium phosphates from seawater solutions, J. Cryst. Growth, 223 (2001) 550–556.
[27] R. Sheikholeslami, Assessment of the scaling potential for sparingly soluble salts in RO and NF units, Desalination, 167 (2004) 247–256.
[28] E. Abdel-Aal, M. Rashad and H. El-Shall, Crystallization of calcium sulfate dihydrate at different supersaturation ratios and different free sulfate concentrations, Cryst. Res. Technol., 39 (2004) 313–321.
[29] K. Al-Anezi, et al., Parameters affecting the solubility of carbon dioxide in seawater at the conditions encountered in MSF desalination plants, Desalination, 222 (2008) 548–571.
[30] D.K. Gledhill and J.W. Morse, Calcite dissolution kinetics in Na–Ca–Mg–Cl brines, Geochim. Cosmochim. Acta, 70 (2006) 5802–5813.
[31] D.K. Gledhill and J.W. Morse, Calcite solubility in Na–Ca–Mg–Cl brines, Chem. Geol., 233 (2006) 249–256.
[32] C. Goyet and A. Poisson, New determination of carbonic acid dissociation constants in seawater as a function of temperature and salinity, Deep sea res., 36(11) (1989) 1635–1654.
[33] P. Zuddas and A. Mucci, Kinetics of calcite precipitation from seawater: I. A classical chemical kinetics description for strong electrolyte solutions, Geochim. Cosmochim. Acta, 58(20) (1994) 4353–4362.
[34] P. Zuddas and A. Mucci, Kinetics of calcite precipitation from seawater: II the influence of the ionic strength, Geochim. et Cosmochim. Acta, 62 (1998) 757–766.
[35] P. Zuddas, K. Pachana and D. Faivre, The influence of dissolved humic acids on the kinetics of calcite precipitation from seawater solutions, Chem. Geol., 201 (2003) 91–101.
[36] H. Elfil and H. Roques, Role of hydrate phases of calcium carbonate on the scaling phenomenon, Desalination, 137 (2001) 177–186.
[37] H. Elfil and H. Roques, Prediction of limit of metastable zone in the $CaCO_3$-CO_2-H_2O system, AIChE J., 50(8) (2004) 1908–1916.
[38] J. Gal, et al., Calcium carbonate solubility: a reappraisal of scale formation and inhibition, Talanta, 43 (1996) 1497–1509.
[39] J. Gal, Y. Fovet and N. Gache, Mechanisms of scale formation and carbon dioxide partial pressure influence.Part II. Application in the study of mineral waters of reference, Water Res., 36 (2002) 764–773.
[40] J.W. Mullin, N. Teodossiev and O. Sohnel, Potassium Sulphate Precipitation from Aqueous Solution by Salting-out with Acetone, Chem. Eng. Process., 26 (1989) 93–99.
[41] E. Dalas, J. Kallitsis and P. Koutsoukos, The crystallization of calcium carbonate on polymeric substrates, J. Cryst. Growth., 89 (1988) 287–294.
[42] H. Yu, The mechanism of composite fouling in Australian sugar mill evaporators by calcium oxalate and amorphous silica, in Chemical Engineering and Industrial chemistry, 2003, University of New South Wales: Sydney.
[43] P. Koutsoukoas and C. Kontoyannis, Precipitation of calcium carbonate in aqueous solutions, J. Chem. Soc., Faraday Trans., 80 (1984) 1181–1192.
[44] J.R. Clarkson, T.J. Price and C.J. Adams, Role of Metastable Phases in the Spontaneous Precipitation of Calcium Carbonate. J. Chem. Soc. Faraday Trans., 88(2) (1992) 243–249.
[45] L. Treccani, Protein Mineral Interaction of Purified Nacre Proteins with Carbonate Crystals, 2006, University of Bremen: Bremen.
[46] E. Dalas, P. Klepetsanis and P.G. Koutsoukos, The Overgrowth of Calcium Carbonate on Poly(vinylchloride-co-vinyl acetate-co-maleic acid), Langmuir, 15 (1999) 8322–8327.
[47] E. Dalas and S. Koklas, The overgrowth of vaterite on functionalized styrene-butadiene copolymer, J. Cryst. Growth, 256 (2003) 401–406.
[48] F. Manoli and E. Dalas, Spontaneous precipitation of calcium carbonate in the presence of ethanol, isopropanol and diethylene glycol, J. Cryst. Growth,. 218 (2000) 359–364.
[49] F. Manoli, et al., The effect of aminoacids on the crystal growth of calcium carbonate, J. Cryst. Growth, 236 (2002) 363–370.
[50] D. Kralj, L. Bre-eviéa and A.E. Nielsen, Vaterite growth and dissolution in aqueous solution II. Kinetics of dissolution, J. Cryst. Growth,. 143 (1994) 269–276.
[51] P.G. Koutsoukos and C.G. Kontoyannis, Prevention and inhibition of calcium carbonate scale, J. Cryst. Growth,. 69 (1984) 367–376.
[52] W. Wu and G.H. Nancollas, The dissolution and growth of sparingly soluble inorganic salts: A kinetics and surface energy approach, Pure Appl. Chem., 70(10) (1998) 1867–1872.
[53] W. Wu and G.H. Nancollas, Determination of interfacial tension from crystallization and dissolution data: a comparison with other methods, Adv. Colloid Interface Sci., 79 (1999) 229–279.
[54] T.G. Sabbides and P.G. Koutsoukos, The crystallization of calcium carbonate in artificial seawater; role of the substrate, J. Cryst. Growth, 133 (1993) 13–22.